



MAPK13 stabilization *via* m⁶A mRNA modification limits anticancer efficacy of rapamycin

Received for publication, January 31, 2023, and in revised form, August 10, 2023. Published, Papers in Press, August 19, 2023.
<https://doi.org/10.1016/j.jbc.2023.105175>

JooHwan Kim¹, Yujin Chun¹, Cuauhtemoc B. Ramirez^{1,2}, Lauren A. Hoffner¹, Sunhee Jung², Ki-Hong Jang¹,
Varvara I. Rubtsova^{2,3}, Cholsoon Jang², and Gina Lee^{1,*}

From the ¹Department of Microbiology and Molecular Genetics, Chao Family Comprehensive Cancer Center, School of Medicine, ²Department of Biological Chemistry, Chao Family Comprehensive Cancer Center, School of Medicine, and ³School of Biological Sciences, University of California Irvine, Irvine, California, USA

Reviewed by members of the JBC Editorial Board. Edited by Alex Tokor

N⁶-adenosine methylation (m⁶A) is the most abundant mRNA modification that controls gene expression through diverse mechanisms. Accordingly, m⁶A-dependent regulation of oncogenes and tumor suppressors contributes to tumor development. However, the role of m⁶A-mediated gene regulation upon drug treatment or resistance is poorly understood. Here, we report that m⁶A modification of mitogen-activated protein kinase 13 (*MAPK13*) mRNA determines the sensitivity of cancer cells to the mechanistic target of rapamycin complex 1 (mTORC1)-targeting agent rapamycin. mTORC1 induces m⁶A modification of *MAPK13* mRNA at its 3' untranslated region through the methyltransferase-like 3 (METTL3)–METTL14–Wilms' tumor 1–associating protein (WTAP) methyltransferase complex, facilitating its mRNA degradation *via* an m⁶A reader protein YTH domain family protein 2. Rapamycin blunts this process and stabilizes *MAPK13*. On the other hand, genetic or pharmacological inhibition of *MAPK13* enhances rapamycin's anticancer effects, which suggests that *MAPK13* confers a progrowth signal upon rapamycin treatment, thereby limiting rapamycin efficacy. Together, our data indicate that rapamycin-mediated *MAPK13* mRNA stabilization underlies drug resistance, and it should be considered as a promising therapeutic target to sensitize cancer cells to rapamycin.

Transcription and translation are central mechanisms to control gene expression. In addition to these canonical processes, cells modify genetic materials with various chemical moieties as an additional layer of gene regulation. While epigenetic modifications of DNA and histones are well established, chemical modifications of RNA (*i.e.*, epitranscriptomic regulation) have been recently shown to play crucial roles in gene regulation (1, 2). Of the mRNA modifications, m⁶A is the most abundant (3). m⁶A is deposited on mRNA by a methyltransferase complex, which is composed of three core proteins: methyltransferase-like 3 (METTL3), METTL14, and Wilms' tumor 1–associating protein (WTAP) (4, 5). m⁶A is mostly enriched on the last exon of mRNA near the stop codon and

3'UTR as revealed by transcriptome-wide sequencing (6, 7). These m⁶A-modified mRNAs then recruit m⁶A-binding “reader” proteins that determine the diverse fates of these mRNAs. For example, the YTHDF (YTH domain family) of m⁶A reader proteins decrease stability or promote the translation efficiency of m⁶A-containing mRNAs (8, 9).

m⁶A-dependent gene regulation is involved in diverse biological processes, such as embryo development, stem cell differentiation, sex determination, and circadian rhythm; dysregulation of this process can cause various diseases including cancers (10–12). Interestingly, both increased and decreased m⁶A levels can lead to cancer development, depending on the downstream target genes. METTL3 overexpression in leukemia cells induces expression of oncogenes such as *cMyc* and *Bcl2* (13). On the other hand, METTL3 downregulation in endometrial cancer induces Akt pro-survival signaling by decreasing the expression of Akt inhibitor, PHLPP2 (PH domain and leucine-rich repeat protein phosphatase 2) (14). Therefore, a comprehensive examination of m⁶A target genes is necessary to better understand the impact of m⁶A modification in different biological and pathological contexts.

As a master regulator of cell growth, mechanistic target of rapamycin complex 1 (mTORC1) is overactivated in most human cancers (15–20). The mTORC1 inhibitor rapamycin was considered as a promising therapeutic agent, but it faced several clinical challenges such as drug resistance or regrowth of tumors after treatment (21–23). It has been suggested that mTORC1-dependent post-translational modification of proteins (*e.g.*, protein phosphorylation) underlie the observed rapamycin resistance mechanisms. However, whether post-transcriptional RNA modifications confer rapamycin resistance is unknown.

Recent work from our and other laboratories revealed that activation of m⁶A mRNA modification by mTORC1 contributes to tumor progression. mTORC1 induces expression of METTL3, METTL14, and WTAP, which methylates and destabilizes the growth-suppressing genes such as *cMyc* suppressor and autophagy genes (24–27). From our transcriptome-wide m⁶A sequencing, we identified additional target genes that are potentially regulated by mTORC1-

* For correspondence: Gina Lee, ginalee@uci.edu.

mTORC1 suppresses progrowth signaling by RNA methylation

dependent m⁶A modification (24). In this study, we report that a mitogen-activated protein kinase (MAPK)/p38 isoform, MAPK13/p38 δ , is a downstream target of the mTORC1–m⁶A RNA modification pathway, which likely contributes to the limited tumor-suppressive effects of rapamycin.

Results

Identification of genes regulated by mTORC1 and m⁶A writer complex

We previously performed m⁶A individual-nucleotide-resolution crosslinking and immunoprecipitation (miCLIP)-Seq in human embryonic kidney 293E (HEK293E) cells, identifying the 17 genes whose m⁶A level is decreased, whereas total mRNA expression is increased by the mTOR catalytic inhibitor, torin1 (24). Since torin1 suppresses both mTORC1 and mTORC2, we then used rapamycin to selectively block mTORC1 and performed quantitative PCR (qPCR) analysis as a secondary screen of candidate genes identified from miCLIP-Seq (Fig. 1A). In parallel, we depleted m⁶A writer complex proteins, METTL3/14 or WTAP, to validate the genes that are regulated by m⁶A modification. For these screens, we used lymphangioliomyomatosis (LAM) 621-101 cell line, a kidney angiomyolipoma cell line isolated from an LAM patient. LAM 621-101 cells have an overactive mTORC1 activity because of a loss of function in the tumor suppressor protein called tuberous sclerosis complex 2 (TSC2) (28, 29). Consistent with our previous findings, inhibition of mTORC1 activity by rapamycin reduced the protein levels of m⁶A writer proteins METTL3, METTL14, and WTAP (Fig. 1, B and C) (24, 25). We found ten genes (*BEX1* [brain expressed X-linked 1], *EIF4A2* [eukaryotic translation initiation factor 4A2], *EIF6* [eukaryotic translation initiation factor 6], *FGFR3* [fibroblast growth factor receptor], *MAPK13*, *NOP56* [NOP56 ribonucleoprotein], *PKD1* [polycystic kidney disease 1], *SLC25A37* [solute carrier family 25 member 37], *STAT5B* [signal transducer and activator of transcription 5B], and *TPR* [translocated promoter region]) whose mRNA levels were elevated by rapamycin (Fig. 1D). *METTL3/14* knockdown increased mRNA levels of *BEX1*, *EIF6*, *MAPK13*, and *SLC25A37* (Fig. 1E), and *WTAP* knockdown increased mRNA levels of *EIF6* and *MAPK13* (Fig. 1F). Analysis of published Gene Expression Omnibus (GEO) dataset (GSE193402) revealed that rapamycin induces mRNA levels of *MAPK13*, *OBSCN* [obscurin], *SLC25A37*, and *STAT5B* in another TSC2-deficient renal angiomyolipoma cell line, UMB1949 (30, 31) (Fig. S1). qPCR analysis further validated *MAPK13* induction upon rapamycin treatment in several mTORC1-overactive cells including UMB1949, MCF7 (PI3K-mutated breast cancer) (32), and BT549 (PTEN-deficient breast cancer) (33) (Fig. 1, G–I). Thus, we decided to further study *MAPK13* based on its dramatic and consistent induction in all conditions across diverse cancer cells.

m⁶A writer complex regulates MAPK13/p38 δ expression among p38 isoforms

Next, we assessed protein levels of MAPK13 to examine whether the changes in *MAPK13* mRNA levels are reflected in MAPK13 protein expression. Upon rapamycin treatment, the

protein levels of MAPK13 increased by twofold (Fig. 2, A and B). Since rapamycin has been shown to suppress both mTORC1 and mTORC2 in some conditions (34–36), we looked at mTORC2 activity using Akt-S473 phosphorylation as a readout. In contrast, the near-complete suppression of mTORC1 activity (measured by pS6-S240/S244) by rapamycin, mTORC2 activity (measured by pAkt-S473) was not inhibited by rapamycin in LAM 621-101 cells (Fig. 2, C and D). Rapamycin rather induced Akt phosphorylation (Fig. 2, C and D), indicating the release of negative feedback suppression of mTORC2 by mTORC1 upon rapamycin treatment (23, 37). Knockdown of *Raptor*, a key component of mTORC1 complex, increased MAPK13 mRNA and protein levels (Fig. 2, E and F), demonstrating mTORC1-dependent regulation of MAPK13 expression. Finally, double knockdown of *METTL3/14* also led to twofold increase in MAPK13 protein expression (Fig. 2, G and H). Overall, the extent of MAPK13 protein induction (Fig. 2, A–H) correlated well with the increase in its mRNA levels (Fig. 1, D–F).

MAPK13 is a member of the p38 MAPK protein family composed of p38 α (MAPK14), p38 β (MAPK11), p38 γ (MAPK12), and p38 δ (MAPK13). These proteins control diverse cellular signaling processes, including proliferation, differentiation, inflammation, and cell death responses (38–42). Interestingly, in contrast to *MAPK13*, knockdown of *METTL3/14* did not induce mRNA expression of *MAPK11*, *MAPK12*, or *MAPK14* (Fig. 2I). In the case of *MAPK11*, its mRNA level was decreased (Fig. 2I). To examine protein level changes of these MAPK isoforms, we used an antibody that detects amino acid sequences across three p38 MAPK isoforms, MAPK11, MAPK12, and MAPK14. This antibody does not detect MAPK13 (43). Interestingly, the protein expression of these p38 isoforms (MAPK11, MAPK12, and MAPK14) did not change regardless of *METTL3/14* knockdown (Fig. 2, J and K). Thus, MAPK13 is a unique p38 isoform suppressed by mTORC1-dependent m⁶A modification.

mTORC1–m⁶A–YTHDF2 destabilizes MAPK13 mRNA

From the analysis of our previous miCLIP-Seq in human HEK293E cells (24), we found an mTORC1-dependent m⁶A modification site on the 3'UTR of *MAPK13* (Fig. 3A). Because some m⁶A modification sites have been shown to be conserved in between human and mouse (6, 7, 44, 45), we investigated whether *MAPK13* m⁶A modification is also conserved in mice. Interestingly, although the mouse *Mapk13* had a well-conserved coding sequence (CDS) with human *MAPK13* (92% homology), the 3'UTR (57.7% homology) and m⁶A site were not conserved in mouse *Mapk13* (Figs. 3A and S2). Rapamycin did not induce *Mapk13* expression in TSC2-deficient mouse kidney tumor cell lines (Fig. 3, B and C), indicating the lack of mTORC1 and m⁶A-dependent MAPK13 regulation mechanisms in mice.

To validate m⁶A-dependent regulation of *MAPK13*, we utilized the mouse *Mapk13* CDS expression construct (42) that is resistant to human *MAPK13* siRNA. This plasmid enabled the expression of *Mapk13* CDS in human cells

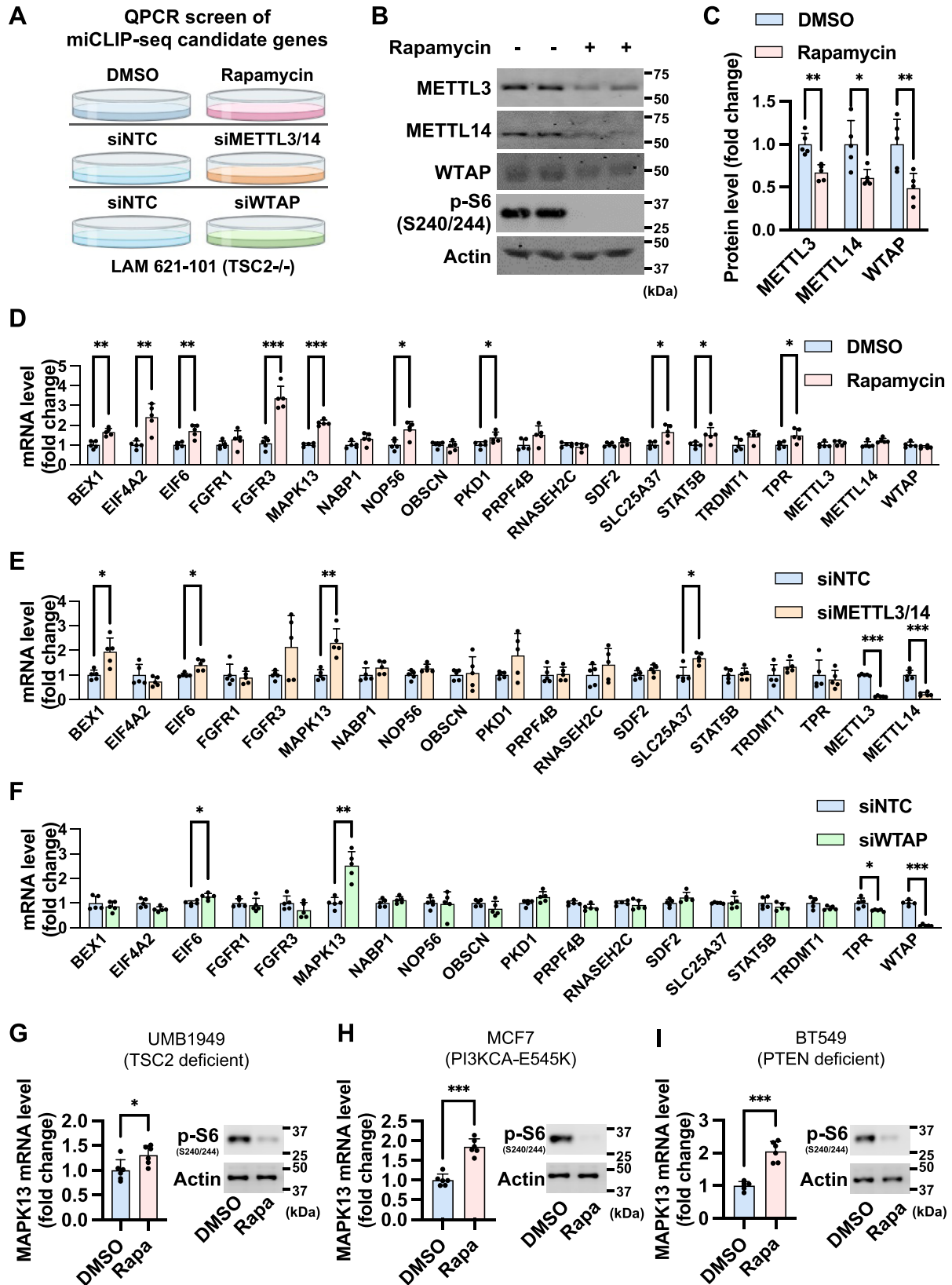


Figure 1. Identification of MAPK13 as the downstream target of rapamycin and m⁶A writer complex. A, schematic of the qPCR screen in LAM 621-101 (TSC2^{-/-}) cells to identify target genes regulated by rapamycin and m⁶A writer complex. The screen sets include three conditions treated with DMSO (control) versus rapamycin for 48 h, transfected with siNTC (control) versus siMETTL3/14, and transfected with siNTC versus siWTAP. Candidate genes were selected from our previous miCLIP-Seq in HEK293E cells treated with mTOR inhibitor, torin1 (24). B and C, immunoblot analysis of LAM 621-101 cells treated with DMSO or rapamycin. C, a quantification graph of immunoblot bands. N = 5. D-F, qPCR analysis of 17 candidate genes in LAM 621-101 cells treated with DMSO versus rapamycin (D), transfected with siNTC versus siMETTL3/14 (E), or transfected with siNTC versus siWTAP (F). N = 5. G-I, qPCR and immunoblot

mTORC1 suppresses progrowth signaling by RNA methylation

knocked down with endogenous *MAPK13* (Fig. 3D). Rapamycin selectively increased expression of the m⁶A site containing endogenous *MAPK13* but not the one that lacks m⁶A modification site (*Mapk13* CDS) (Fig. 3, D and E). Furthermore, a luciferase assay revealed that abrogation of the m⁶A modification site (A1212 to T mutation) increases expression of *MAPK13* 3'UTR luciferase reporter (Fig. 3, A and F). These results indicate that m⁶A modification on *MAPK13* 3'UTR decreases its expression, and rapamycin reverses this regulatory process by suppressing the mTORC1-dependent m⁶A modification.

Once modified with m⁶A, mRNAs recruit m⁶A reader proteins that determine the fate of target transcripts such as changes in mRNA stability or translation efficiency (8, 9). Given that suppression of such m⁶A modification on *MAPK13* by *METTL3/14* or *WTAP* knockdown increases both *MAPK13* mRNA and protein levels (Figs. 1 and 2), we hypothesized that *MAPK13* mRNA is degraded by YTHDF2, an m⁶A reader protein that destabilizes target transcripts (8, 9, 46, 47). Consistent with our hypothesis, knockdown of *YTHDF2* resulted in a significant increase in *MAPK13* mRNA levels (Fig. 3G). Consequently, *MAPK13* protein levels also increased (Fig. 3H). Hence, YTHDF2 is the effector protein responsible for *MAPK13* mRNA degradation upon mTORC1-mediated m⁶A modification.

To further verify whether the stability of *MAPK13* mRNA is indeed regulated by mTORC1-dependent m⁶A modification, we assessed mRNA half-life. To this end, we treated several cancer cell lines with actinomycin D to block *de novo* mRNA synthesis and measured the remaining transcript levels at different time points (48). In the vehicle-treated control condition, *MAPK13* mRNA was degraded in a time-dependent manner with a half-life of 6 to 8 h (Fig. 3I). However, upon rapamycin treatment, the stability of *MAPK13* mRNA was dramatically increased, with 75 to 90% of transcripts remaining even after 8 h (Fig. 3I). Similarly, *METTL3/14* double knockdown also markedly increased the half-life of *MAPK13* mRNA but not that of the other three p38 isoforms (Fig. 3, J–M). Collectively, these results demonstrate that rapamycin increases mRNA stability of *MAPK13* via the m⁶A–YTHDF2 axis.

MAPK13 inhibition enhances rapamycin's anticancer effect

Among the various MAPK family proteins, MAPK13 has been shown to contribute to tumor progression and inflammatory responses (38–42, 49). One such MAPK13 downstream is the eukaryotic elongation factor-2 kinase (eEF2K)–eEF2 pathway. eEF2 is a translation elongation factor that promotes translocation of peptidyl-tRNA in ribosomes, whereas eEF2K is a negative regulator of protein translation by suppressing eEF2 activity through eEF2–T56 phosphorylation

(49, 50). MAPK13 phosphorylates eEF2K at Ser359 and inhibits its activity, which results in decreased eEF2 phosphorylation and enhanced protein synthesis (51, 52). Consistent with the previous reports, *MAPK13* knockdown increased eEF2–T56 phosphorylation (Figs. 4A and S3A), reflecting the enhanced eEF2K activity upon MAPK13 inhibition. It is noteworthy that eEF2K can also be suppressed by mTORC1 and its downstream effector S6K (53). Consequently, rapamycin treatment led to eEF2 phosphorylation. However, when we knocked down *MAPK13* in rapamycin-treated cells, eEF2–T56 phosphorylation was further enhanced (Fig. 4A), indicating that the increased expression of MAPK13 was limiting the extent of eEF2K-dependent eEF2 phosphorylation in rapamycin-treated cells.

Next, we examined the impact of rapamycin–MAPK13 signaling in cell proliferation and survival. Even though the single treatment of rapamycin or *MAPK13* knockdown reduced the proliferation of mTORC1-hyperactive cancer cells including LAM 621-101, UMB1949, and MCF7, rapamycin was more effective in cell growth suppression when MAPK13 was depleted (Fig. 4, B–D). Rapamycin-mediated cell migration suppression was also further enhanced by *MAPK13* knockdown (Fig. 4, E and F). Finally, a small molecule inhibitor of MAPK13, MAPK13-IN-1 (54, 55), also showed a synergistic effect with rapamycin in suppressing cell growth (Figs. 4, G and H and S3B). Together, these findings indicate that MAPK13 induction by rapamycin limits the tumor-suppressive effects of rapamycin, and the combinatory treatment of rapamycin with MAPK13 inhibitor can be more effective in impairing tumor growth compared with the rapamycin monotherapy (Fig. 4I).

Discussion

Because of rapamycin's specific inhibitory activity on mTORC1, it was initially discussed as a ground-breaking anti-cancer therapeutic for a broad spectrum of mTORC1-overactivated human cancers. However, clinical trials revealed that rapamycin was not as efficient as expected. Some tumors even regrow into a bigger size after cessation of rapamycin treatment, and sustained rapamycin therapies generate significant toxicities in some patients (21–23). One of the mechanisms for rapamycin resistance is activation of other growth-promoting signaling pathways (56, 57). In breast cancer patients, mitogenic extracellular signal-regulated kinase –MAPK signaling was increased in cancer tissues upon rapamycin treatment (58). This unexpected observation led to the identification of negative feedback signaling pathways downstream of mTORC1; while mTORC1 promotes anabolic pathways for cell growth, it ironically inhibits several progrowth signals including PI3K, Ras, and MEK (23). Some of these progrowth signals such as PI3K and RAS are upstream activators of mTORC1;

analyses of UMB1949 (G), MCF7 (H), and BT549 (I) cells treated with DMSO or rapamycin. **p* < 0.05, ***p* < 0.01, ****p* < 0.001. Error bars show SD. Numbers on the immunoblot indicate the positions of molecular weight markers. See also Fig. S1. DMSO, dimethyl sulfoxide; HEK293E, human embryonic kidney 293E cell line; LAM, lymphangioleiomyomatosis; m⁶A, N⁶-adenosine methylation; *MAPK13*, mitogen-activated protein kinase 13; *METTL*, methyltransferase-like protein; miCLIP, m⁶A individual-nucleotide-resolution crosslinking and immunoprecipitation; mTOR, mechanistic target of rapamycin; qPCR, quantitative PCR; TSC2, tuberous sclerosis complex 2; *WTAP*, Wilms' tumor 1–associating protein.

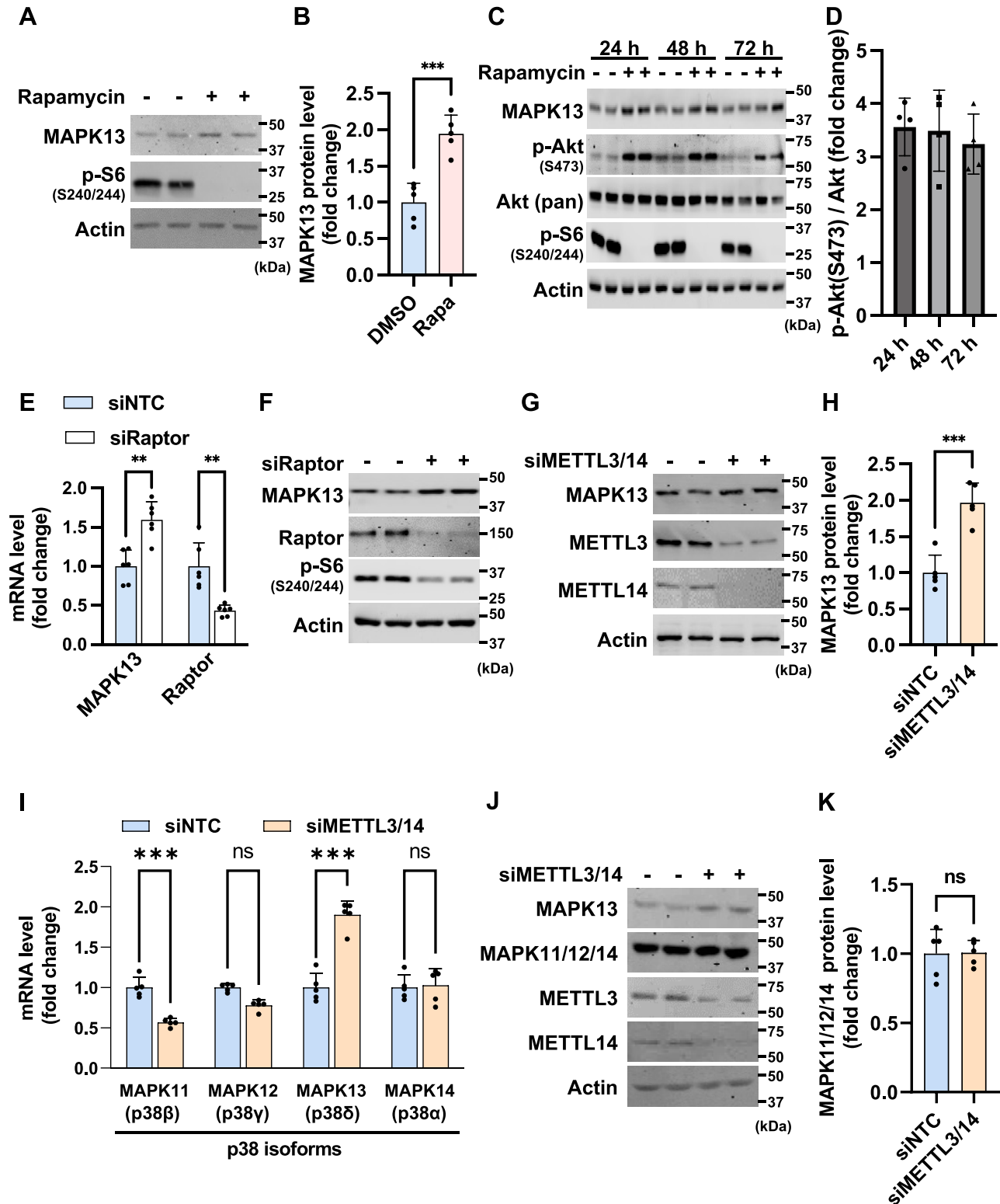


Figure 2. mTORC1 and m⁶A regulate MAPK13/p38 δ expression among p38 MAPK isoforms. *A* and *B*, immunoblot analysis of LAM 621-101 cells treated with DMSO or rapamycin. *B*, the quantification graph of immunoblot bands. *N* = 5. *C* and *D*, immunoblot analysis of LAM 621-101 cells treated with rapamycin in time course. *D*, a quantification graph of immunoblot bands. *N* = 5. *E* and *F*, qPCR analysis (*E*) and immunoblot analysis (*F*) of LAM 621-101 cells transfected with siNTC or siRaptor. *N* = 5. *G* and *H*, immunoblot analysis of LAM 621-101 cells transfected with siNTC or siMETTL3/14. *H*, a quantification graph of immunoblot bands. *N* = 5. *I*, qPCR analysis of p38 MAPK family genes. LAM 621-101 cells were transfected with siNTC or siMETTL3/14. *N* = 5. *J* and *K*, immunoblot analysis of LAM 621-101 cells transfected with siNTC or siMETTL3/14. *J*, a quantification graph of immunoblot bands. *N* = 5. ****p* < 0.001, ns = not significant. Error bars show SD. Numbers on the immunoblot indicate the positions of molecular weight markers. DMSO, dimethyl sulfoxide; LAM, lymphangioleiomyomatosis; m⁶A, N⁶-adenosine methylation; MAPK13, mitogen-activated protein kinase 13; mTORC1, mechanistic target of rapamycin complex 1; qPCR, quantitative PCR.

mTORC1 suppresses progrowth signaling by RNA methylation

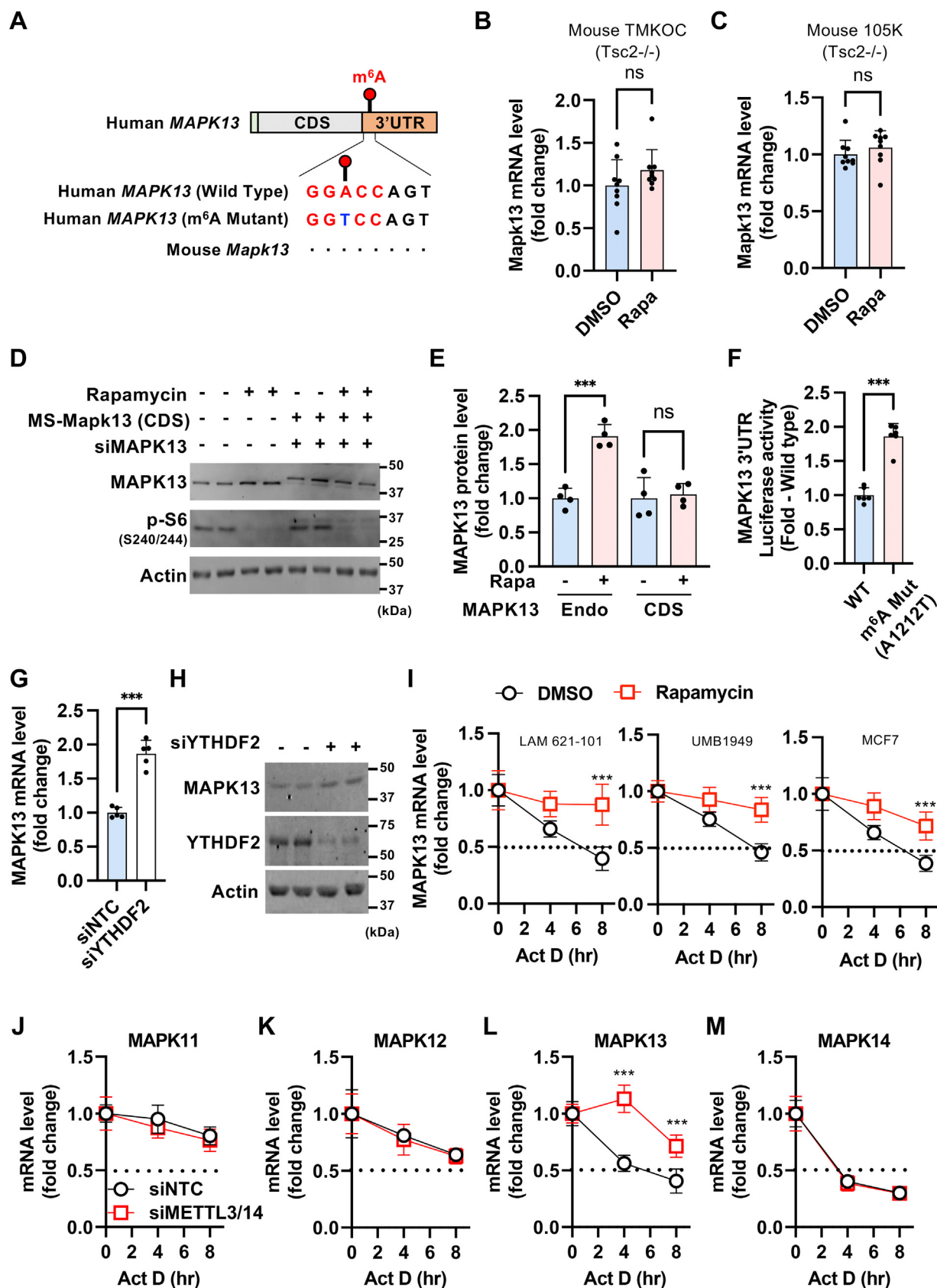


Figure 3. *MAPK13* mRNA stability is regulated by mTORC1–m⁶A–YTHDF2 axis. **A**, schematic of human *MAPK13* mRNA containing m⁶A modification site on the 3'UTR. Sequence alignment analysis revealed that the m⁶A modification site is not conserved in mouse *Mapk13*. Detailed sequence conservation analysis is shown in Fig. S2. In the m⁶A mutant construct, A1212 was mutated to T in the 3'UTR of human *MAPK13*. **B** and **C**, qPCR analysis of *Mapk13* mRNA levels in mouse TMKOC (**B**) and 105K (**C**) cells treated with DMSO or rapamycin. N = 9. **D** and **E**, immunoblot analysis of LAM 621-101 cells treated with DMSO or rapamycin. Endogenous *MAPK13* (Endo) was knocked down with siRNA, and siRNA-resistant mouse *Mapk13* (CDS) was ectopically expressed. **E**,

therefore, when mTORC1 is suppressed by rapamycin, these negative feedbacks are released, resulting in the continued growth of cancer cells (59). On the other hand, cotreatment of rapamycin with PI3K or MEK inhibitors is more effective for tumor suppression in cell culture and mouse models (58, 60). Here, we identified MAPK13 as a target gene regulated by mTORC1-dependent m⁶A regulation and as another key factor that potentially limits rapamycin's tumor-suppressive effects. MAPK13 has been shown to activate mTORC1, indicating a potential negative feedback loop between MAPK13 and mTORC1 (61). Indeed, genetic knockdown or pharmacological inhibition of MAPK13 in combination with rapamycin enhanced rapamycin's effect on cell growth and migration suppression, suggesting MAPK13 as a promising therapeutic target for augmenting rapamycin sensitivity (Fig. 4).

In the basal state of mTORC1-overactive cells, *MAPK13* mRNA undergoes destabilization because of mTORC1-dependent m⁶A modification. However, mRNA destabilization does not completely deplete *MAPK13*, in contrast to the near-complete removal of *MAPK13* mRNA by siRNA treatment (Fig. S3A). Subsequently, these residual *MAPK13* mRNAs produce MAPK13 proteins. Through a cycloheximide protein stability assay, we found that MAPK13 protein exhibits remarkable stability, with a half-life exceeding 24 h. This is in stark contrast to the positive control of cycloheximide assay, cMYC, which displays a half-life of less than 1 h (Fig. S3, C and D). Building upon this observation, we propose that MAPK13 proteins synthesized from the residual *MAPK13* mRNAs maintain a minimal yet significant level of MAPK13 signaling activity under basal conditions (Fig. 4I, left). This model is further supported by the fact that genetic knockdown or small-molecule inhibitor of MAPK13 diminishes cell proliferation and attenuates MAPK13 downstream signaling (Fig. 4, A and G). On the other hand, upon rapamycin treatment, the stabilized *MAPK13* mRNAs produce even more MAPK13 proteins, which facilitates MAPK13-dependent progrowth signaling (Fig. 4I, middle). Consequently, inhibition of MAPK13 activity in conjunction with rapamycin offers the most effective tumor suppression (Fig. 4I, right).

MAPK13 is one of the four p38 MAPK family proteins. Among the isoforms, MAPK14/p38 α and MAPK11/p38 β are expressed in most cell types, whereas the other MAPK family genes are expressed in specific tissues; MAPK12/p38 γ is expressed in the skeletal muscle, whereas MAPK13/p38 δ is expressed in the kidney and lung (41, 62). Intriguingly, the kidney and lung are the two dominant organs that develop tumors in TSC and LAM patients with overactive mTORC1 activity (63). Our data indicate that, among the p38 MAPK family genes, only MAPK13/p38 δ

was regulated by mTORC1-dependent m⁶A modification (Figs. 2 and 3). Therefore, small-molecule inhibitors that specifically target MAPK13/p38 δ isoform such as MAPK13-IN-1 can be a selective therapeutic regimen with improved efficacy and lower toxicity. While p38 α /MAPK14 isoform has been most extensively studied, p38 δ /MAPK13 has recently emerged as a potential drug target because of its roles in stress responses, cytokine production, and tumor development (39, 40, 55, 64). Our findings therefore highlight MAPK13 as a promising target for combination therapy with rapamycin to overcome the limited tumor suppression efficacy of rapamycin.

Experimental procedures

Cell culture and drug treatment

TSC2-deficient kidney tumor cell lines, LAM 621-101 (human, Research Resource Identifier [RRID]: CBCL_S897) (28), 105K (mouse) (65), and TMKOC (mouse) (66), were provided by Drs Jane Yu and Elisabeth Henske. TMKOC was originally generated by Dr Vera Krymskaya (67). HEK293E cell line (RRID: CVCL_6974), MCF7 (RRID: CVCL_0031), BT549 (RRID: CVCL_1092), and UMB1949 (RRID: CVCL_C471) were obtained from American Type Culture Collection. LAM 621-101, UMB1949, MCF7, BT549, TMKOC, 105K, and HEK293E cells were grown in Dulbecco's modified Eagle's medium (GIBCO) with 10% fetal bovine serum (FBS) (Sigma–Aldrich) at 37 °C with 5% CO₂. About 5 × 10⁶ cells counted by Multisizer 4e Coulter Counter (Beckman) were plated on a 60 mm plate and serum starved for 24 h unless otherwise indicated. Rapamycin (Calbiochem) dissolved in dimethyl sulfoxide (DMSO) was treated at the final concentration of 20 nM (LAM 621-101, UMB1949, MCF7, and BT549) or 100 nM (TMKOC and 105K). MAPK13-IN-1 (MAPK13 inhibitor; MedChemExpress) dissolved in DMSO was treated at the final concentration of 5 μ M unless otherwise indicated.

Transfection of DNA and siRNA

siRNAs (Sigma–Aldrich) dissolved in nuclease-free water were transfected into cells using Lipofectamine RNAiMAX reagent (Invitrogen) at the final concentration of 30 nM. siRNA list is provided in Table S1. For expression of the human siRNA-resistant mouse *Mapk13* plasmid, pCDNA3-FLAG-*Mapk13* (Addgene; catalog no.: 20785) (57) was transfected using FuGENE HD (Promega) 2 days before siRNA transfection.

Cell proliferation assay

siRNA-transfected cells were seeded on a 60 mm plate. After 24 h, cells were treated with DMSO (control) or

quantification of MAPK13 protein expression normalized to DMSO-treated group in each condition. N = 4. F, luciferase activity of *MAPK13* 3'UTR renilla luciferase reporters containing WT or mutant (m⁶A Mut, A1212T) m⁶A sites. The renilla luciferase activity was normalized to control cyprid luciferase activity. N = 6. G and H, qPCR (N = 5) (G) and immunoblot analysis (H) of LAM 621-101 cells transfected with siNTC or siYTHDF2. I, mRNA stability analysis of *MAPK13* in LAM 621-101, UMB1949, and MCF7 cells treated with rapamycin. Cells were treated with actinomycin D for the indicated times, and qPCR was performed to measure the remaining mRNA level. N = 5. J–M, mRNA stability analysis of p38 isoform in LAM 621-101 cells transfected with siNTC or siMETTL3/14. Cells were treated with actinomycin D for the indicated times, and qPCR was performed to measure the remaining mRNA level. N = 5. **p* < 0.05, ***p* < 0.01, ****p* < 0.001. Error bars show SD. Numbers on the immunoblot indicate the positions of molecular weight markers. See also Fig. S2. 3'UTR, 3' untranslated region; CDS, coding sequence; DMSO, dimethyl sulfoxide; m⁶A, N⁶-adenosine methylation; MAPK13, mitogen-activated protein kinase 13; mTORC1, mechanistic target of rapamycin complex 1; qPCR, quantitative PCR; YTHDF2, YTH domain family protein 2.

mTORC1 suppresses progrowth signaling by RNA methylation

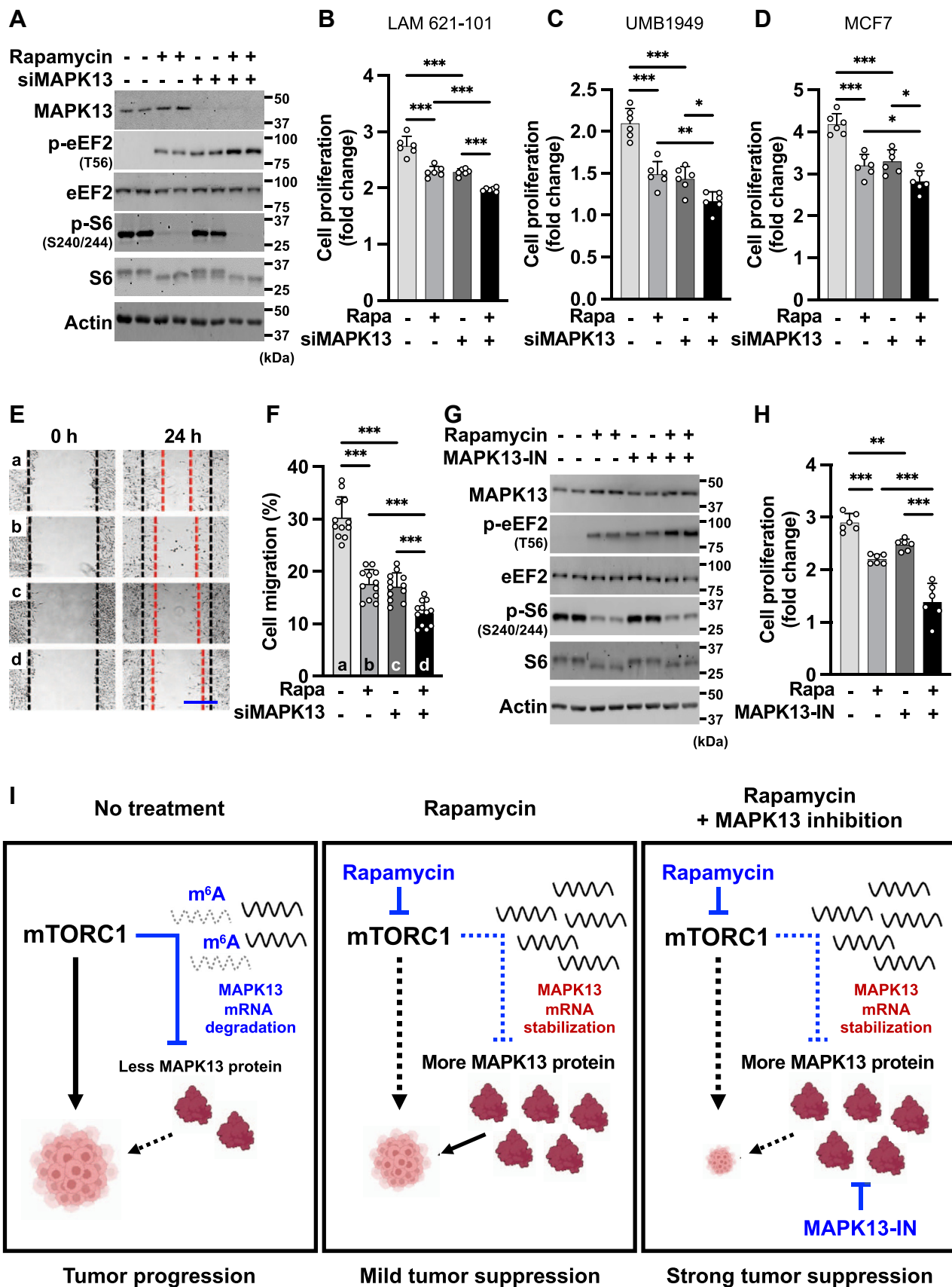


Figure 4. MAPK13 inhibition enhances rapamycin's suppressive effect on cell growth and migration. A, immunoblot analysis of LAM 621-101 cells transfected with siNTC or siMAPK13 in combination with DMSO or rapamycin treatment. B–D, cell proliferation assay of LAM 621-101 (B), UMB1949 (C), and MCF7 (D) cells transfected with siNTC or siMAPK13 in combination with DMSO or rapamycin. The graph shows the fold increase in cell numbers 3 days after

rapamycin without FBS. For cotreatment of MAPK13 inhibitor with rapamycin, MAPK13-IN-1 was pretreated 1 h before rapamycin unless otherwise indicated. Cell numbers were measured using Multisizer 4e Coulter Counter (Beckman) at 0 and 72 h after treatment. Cell proliferation (fold change) was calculated by dividing the cell numbers at 72 h by the cell numbers at 0 h.

Cell migration assay

Wound-healing assay was applied to assess cell migration. siRNA-transfected cells were seeded on a 6-well plate. After 24 h, cells were treated with DMSO (control) or rapamycin without FBS. Once cells are confluent, a clear wound line was created using a sterile 200 μ l pipette tip. Cell images containing the wound area were taken at 0 and 24 h using Eclipse Ts2-FL microscope and DS-Fi3 Camera (Nikon). Cell migration efficiency (%) was calculated by measuring the cell migration area (0–24 h) using the ImageJ software program (NIH).

Crystal violet assay

Cells grown on 12-well plates were fixed with 4% methanol-free formaldehyde (Polysciences) and incubated with 0.1% crystal violet solution (Sigma–Aldrich) for 30 min. After rinsing five times with PBS, the plates were scanned for image analysis. For quantification, crystal violet dyes were eluted from the cells using methanol, and the absorbance of crystal violet solution was measured at 570 nm using Victor Nivo plate reader (PerkinElmer).

Immunoblot

Cells were homogenized on ice using radio-immunoprecipitation assay lysis buffer (25 mM Tris–HCl [pH 7.4], 2 mM EDTA, 150 mM NaCl, 0.1% SDS, 2 mM DTT, 1% sodium deoxycholate, and 1% NP-40) supplemented with protease inhibitors (1 mM PMSF, 2 μ g/ml pepstatin A, 10 μ g/ml leupeptin, and 10 μ g/ml aprotinin) and phosphatase inhibitors (10 mM NaF and 1 mM Na_3VO_4). Cell lysates were cleared by centrifugation at 13,000 rpm at 4 °C for 30 min. Detergent-compatible protein assay (Bio-Rad) was used to measure protein concentration. Proteins were boiled for 10 min with Laemmli sample buffer. SDS-PAGE gels were used to separate proteins (10–30 μ g) and transferred to the nitrocellulose membrane (Amersham Biosciences). Membranes were then incubated with Odyssey blocking solution (Li-COR Biosciences), followed by incubation with primary and IRDye secondary antibodies (Li-COR Biosciences). Immunoblot signals were detected and quantified by Image

Studio software with the Li-COR imaging system (Li-COR Biosciences). Immunoblot images are representative of at least two independent experiments. Primary antibodies against p-S6(S240/S244) (catalog no.: 2211), S6 (catalog no.: 2317), beta-actin (catalog no.: 3700), p38 (MAPK11/12/14) (catalog no.: 8690), METTL3 (catalog no.: 86132), METTL14 (catalog no.: 51104), Pan-Akt (catalog no.: 4691), p-Akt (S473) (catalog no.: 4060), eEF2 (catalog no.: 2332), p-eEF2 (T56) (catalog no.: 2331), YTHDF2 (catalog no.: 71283) and cMyc (catalog no.: 5605) (Cell Signaling Technology); WTAP (catalog no.: Ab195380) (Abcam); and MAPK13 (catalog no.: AF1519) (R&D Systems) were used.

Protein stability analysis

Cells were treated with 50 μ g/ml cycloheximide (Sigma–Aldrich) to inhibit translation, and cell lysates were collected at 0, 1, 2, 4, 6, 12, and 24 h to analyze the remaining protein levels. Protein expression was analyzed by immunoblot assay as described previously.

qPCR

PureLink RNA isolation kit (Life Technologies) was used to isolate total RNA from cells. After removing genomic DNA by DNase I (Sigma–Aldrich), RNA was reverse transcribed to complementary DNA using the iScript kit (Bio-Rad). The resulting complementary DNA was analyzed by qRT–PCR using SYBR Green Master Mix (Life Technologies) on QuantStudio6 Real-Time PCR system (Life Technologies). For the qPCR screen in Figure 1, 17 final candidate genes from our previous miCLIP-Seq performed in HEK293E cells with and without mTOR inhibitor, torin1, were used (24). mRNA levels were calculated by delta–delta CT method using housekeeping genes *ACTIN*, *PPIB*, and *TBP* (human), or *Actin*, *Tbp*, and *36B4* (mouse). The primer list is provided in Table S2.

mRNA stability analysis

Cells were treated with 5 μ g/ml actinomycin D (Sigma–Aldrich) to inhibit transcription and collected at 0, 4, and 8 h to analyze the remaining mRNA levels. Total RNA was extracted, and mRNA levels were analyzed by qPCR as described previously.

Luciferase reporter assay

HEK293E cells were seeded on a 12-well plate. After 24 h, 500 ng of renilla (Switchgear Genomics S805935 MAPK13 3'UTR or MAPK13 m⁶A site mutant constructs) and 100 ng of cypridina (Switchgear Genomics SN0322S) luciferase constructs were cotransfected into cells using FuGENE HD

drug treatment. N = 6. E and F, wound healing assay of LAM 621-101 cells transfected with siNTC or siMAPK13 in combination with DMSO or rapamycin. After scratching the cell layer to form a wound, images were captured at 0 and 24 h to assess cell migration. Black dotted lines indicate the initial wound area at 0 h; red dotted lines mark the migrating front of cells at 24 h (E). Cell migration efficiency was calculated by measuring the wound area at each time point by ImageJ software (F). Scale bar represents 500 μ m. N = 12. G and H, immunoblot (G) and cell proliferation (H) analysis of LAM 621-101 cells treated with MAPK13-IN (MAPK13-IN-1, MAPK13 inhibitor) with or without rapamycin. The graph in (H) shows relative fold increase in cell numbers 3 days after drug treatment. N = 6. I, a schematic diagram describing the regulation of MAPK13 expression by mTORC1-dependent m⁶A methylation (left, without rapamycin; middle, with rapamycin) and the synergistic effect of MAPK13 inhibition in tumor suppression in combination with rapamycin treatment (right). **p* < 0.05, ***p* < 0.01, ****p* < 0.001. Error bars show SD. Numbers on the immunoblot indicate the positions of molecular weight markers. See also Fig. S3; DMSO, dimethyl sulfoxide; MAPK13, mitogen-activated protein kinase 13; mTORC1, mechanistic target of rapamycin complex 1.

mTORC1 suppresses progrowth signaling by RNA methylation

(Promega). About 48 h after transfection, luciferase activity was measured using LightSwitch Renilla Luciferase Assay reagent (Switchgear Genomics) and Pierce Cypridina Luciferase Glow Assay kit (Pierce) on Victor Nivo plate reader (PerkinElmer) according to the manufacturer's protocols. The activity of renilla luciferase was normalized by cypridina luciferase activity.

Site-directed mutagenesis

The point mutation of m⁶A modification site (A1212 to T1212) of human MAPK13 3'UTR luciferase reporter (Switchgear Genomics S805935) was generated using a QuickChange site-directed mutagenesis kit according to the manufacturer's protocol using Pfu Ultra polymerase (Agilent Technologies). Mutagenesis primers are MAPK13-3UTR-GGACC-mut-fw (5'-CACTGCCCAAGGTCAGTATTTGTC-3') and MAPK13-3UTR-GGACC-mut_rv (5'-GACAAATACTGGACCTTGGG CAGTG-3').

Analysis of sequence conservation

CDS and 3'UTR sequences of *MAPK13* were obtained from the National Center for Biotechnology Information database: human (NM_002754.5) and mouse (NM_011950.2). Sequence alignment was performed using Clustal Omega (EMBL-EBI).

GEO dataset analysis

RNA-Seq results of rapamycin-treated UMB1949 cells were obtained from public dataset (GEO accession number: GSE193402). The raw fastq files were mapped to Ensembl human genome assembly GRCh38.107 using the STAR aligner (version 2.7.10b). Raw counts calculated from featureCounts (version 2.0.3) were used as inputs for Deseq2 (version 1.34) for the differential gene expression analysis.

Statistical analysis

Statistical analyses were performed using GraphPad Prism software (GraphPad Software, Inc). All values are presented as mean \pm SD. Statistical significance was determined using a two-tailed Student's *t* test for comparison between two. Statistical significance is presented as **p* < 0.05, ***p* < 0.01, ****p* < 0.001, or ns = not significant.

Data availability

All data are included within the article and [Supporting information](#). The materials and methods in this study are available from the corresponding author upon request.

Supporting information—This article contains supporting information (24).

Acknowledgments—We are grateful to Drs Jane Yu, Elisabeth Henske, and Roger Davis for sharing cell lines and plasmids. We thank Drs John Blenis, David Fruman, Minji Byun, Yongsheng Shi, and members of the Lee and Jang laboratories for technical assistance and scientific discussions. We also would like to acknowledge

the support of the Chao Family Comprehensive Cancer Center Genomics Research and Technology Hub Shared Resource. Schematics in the figures are created with BioRender.

Author contributions—J. K., Y. C., C. J., and G. L. conceptualization; J. K., Y. C., C. B. R., L. A. H., S. J., K.-H. J., and V. I. R. methodology; J. K. and Y. C. investigation; J. K., Y. C., C. J., and G. L. writing—original draft; C. B. R., L. A. H., S. J., K.-H. J., and V. I. R. writing—review & editing; C. J. and G. L. supervision.

Funding and additional information—This research was supported by Department of Defense TS200022 (to G. L.), National Institutes of Health K22CA234399 (to G. L.), Mary Kay Ash Foundation (to G. L.), R01AA029124 (to C. J.), and P30CA062203 (University of California Chao Family Comprehensive Cancer Center). C. B. R. was supported by predoctoral fellowships from the University of California Initiative for Maximizing Student Development (R25GM055246) and Interdisciplinary Cancer Research (T32CA009054) programs. S. J. was supported by a postdoctoral fellowship from the National Research Foundation of Korea (grant no.: 2021R1A6A3A14039681). The content is solely the responsibility of the authors and does not necessarily represent the official views of the National Institutes of Health.

Conflict of interest—The authors declare that they have no conflicts of interest with the contents of this article.

Abbreviations—The abbreviations used are: CDS, coding sequence; DMSO, dimethyl sulfoxide; eEF2K, eukaryotic elongation factor-2 kinase; FBS, fetal bovine serum; GEO, Gene Expression Omnibus; HEK293E, human embryonic kidney 293E cell line; LAM, lymphangioleiomyomatosis; m⁶A, N⁶-adenosine methylation; MAPK13, mitogen-activated protein kinase 13; MAPK13-IN, MAPK13 inhibitor; METTL, methyltransferase-like protein; miCLIP, m6A individual-nucleotide-resolution crosslinking and immunoprecipitation; mTORC1, mechanistic target of rapamycin complex 1; qPCR, quantitative PCR; RRID, Research Resource Identifier; TSC2, tuberous sclerosis complex 2; WTAP, Wilms' tumor 1-associating protein; YTHDF2, YTH domain family protein 2.

References

1. Fu, Y., Dominissini, D., Rechavi, G., and He, C. (2014) Gene expression regulation mediated through reversible m6A RNA methylation. *Nat. Rev. Genet.* **15**, 293–306
2. Frye, M., Jaffrey, S. R., Pan, T., Rechavi, G., and Suzuki, T. (2016) RNA modifications: what have we learned and where are we headed? *Nat. Rev. Genet.* **17**, 365–372
3. Desrosiers, R., Friderici, K., and Rottman, F. (1974) Identification of methylated nucleosides in messenger RNA from Novikoff hepatoma cells. *Proc. Natl. Acad. Sci. U. S. A.* **71**, 3971–3975
4. Karthiya, R., and Khandelia, P. (2020) m6A RNA methylation: ramifications for gene expression and human health. *Mol. Biotechnol.* **62**, 467–484
5. Huang, H., Weng, H., and Chen, J. (2020) m6A modification in coding and non-coding RNAs: roles and therapeutic implications in cancer. *Cancer Cell* **37**, 270–288
6. Meyer, K. D., Saletore, Y., Zumbo, P., Elemento, O., Mason, C. E., and Jaffrey, S. R. (2012) Comprehensive analysis of mRNA methylation reveals enrichment in 3' UTRs and near stop codons. *Cell* **149**, 1635–1646
7. Dominissini, D., Moshitch-Moshkovitz, S., Schwartz, S., Salmon-Divon, M., Ungar, L., Osenberg, S., et al. (2012) Topology of the human and mouse m6A RNA methylomes revealed by m6A-seq. *Nature* **485**, 201–206
8. Zaccara, S., and Jaffrey, S. R. (2020) A unified model for the function of YTHDF proteins in regulating m6A-modified mRNA. *Cell* **181**, 1582–1595.e18

9. Lee, Y., Choe, J., Park, O. H., and Kim, Y. K. (2020) Molecular mechanisms driving mRNA degradation by m6A modification. *Trends Genet.* **36**, 177–188
10. Wu, J., Frazier, K., Zhang, J., Gan, Z., Wang, T., and Zhong, X. (2020) Emerging role of m6A RNA methylation in nutritional physiology and metabolism. *Obes. Rev.* **21**, e12942
11. Wang, T., Kong, S., Tao, M., and Ju, S. (2020) The potential role of RNA N6-methyladenosine in cancer progression. *Mol. Cancer* **19**, 88
12. Jaffrey, S. R., and Kharas, M. G. (2017) Emerging links between m6A and misregulated mRNA methylation in cancer. *Genome Med.* **9**, 2
13. Vu, L. P., Pickering, B. F., Cheng, Y., Zaccara, S., Nguyen, D., Minuesa, G., et al. (2017) The N6-methyladenosine (m6A)-forming enzyme METTL3 controls myeloid differentiation of normal hematopoietic and leukemia cells. *Nat. Med.* **23**, 1369–1376
14. Liu, J., Eckert, M. A., Harada, B. T., Liu, S.-M., Lu, Z., Yu, K., et al. (2018) m6A mRNA methylation regulates AKT activity to promote the proliferation and tumorigenicity of endometrial cancer. *Nat. Cell Biol.* **20**, 1074–1083
15. Menon, S., and Manning, B. D. (2008) Common corruption of the mTOR signaling network in human tumors. *Oncogene* **27**, S43–S51
16. Zou, Z., Tao, T., Li, H., and Zhu, X. (2020) mTOR signaling pathway and mTOR inhibitors in cancer: progress and challenges. *Cell Biosci.* **10**, 31
17. Mossmann, D., Park, S., and Hall, M. N. (2018) mTOR signalling and cellular metabolism are mutual determinants in cancer. *Nat. Rev. Cancer* **18**, 744–757
18. Kim, J., and Guan, K.-L. (2019) mTOR as a central hub of nutrient signalling and cell growth. *Nat. Cell Biol.* **21**, 63–71
19. Liu, G. Y., and Sabatini, D. M. (2020) mTOR at the nexus of nutrition, growth, ageing and disease. *Nat. Rev. Mol. Cell Biol.* **21**, 183–203
20. Foster, D. A., Salloum, D., Menon, D., and Frias, M. A. (2014) Phospholipase D and the maintenance of phosphatidic acid levels for regulation of mammalian target of rapamycin (mTOR). *J. Biol. Chem.* **289**, 22583–22588
21. Bissler, J. J., McCormack, F. X., Young, L. R., Elwing, J. M., Chuck, G., Leonard, J. M., et al. (2008) Sirolimus for angiomyolipoma in tuberous sclerosis complex or lymphangiomyomatosis. *N. Engl. J. Med.* **358**, 140–151
22. Marsh, D. J., Trahair, T. N., Martin, J. L., Chee, W. Y., Walker, J., Kirk, E. P., et al. (2008) Rapamycin treatment for a child with germline PTEN mutation. *Nat. Clin. Pract. Oncol.* **5**, 357–361
23. Li, J., Kim, S. G., and Blenis, J. (2014) Rapamycin: one drug, many effects. *Cell Metab.* **19**, 373–379
24. Cho, S., Lee, G., Pickering, B. F., Jang, C., Park, J. H., He, L., et al. (2021) mTORC1 promotes cell growth via m6A-dependent mRNA degradation. *Mol. Cell* **81**, 2064–2075.e8
25. Tang, H.-W., Weng, J.-H., Lee, W. X., Hu, Y., Gu, L., Cho, S., et al. (2021) mTORC1-chaperonin CCT signaling regulates m6A RNA methylation to suppress autophagy. *Proc. Natl. Acad. Sci. U. S. A.* **118**, e2021945118
26. Villa, E., Sahu, U., O'Hara, B. P., Ali, E. S., Helmin, K. A., Asara, J. M., et al. (2021) mTORC1 stimulates cell growth through SAM synthesis and m⁶A mRNA-dependent control of protein synthesis. *Mol. Cell* **81**, 2076–2093.e9
27. Jang, K.-H., Heras, C. R., and Lee, G. (2022) m6A in the signal transduction network. *Mol. Cells* **45**, 435–443
28. Yu, J., Astrinidis, A., Howard, S., and Henske, E. P. (2004) Estradiol and tamoxifen stimulate LAM-associated angiomyolipoma cell growth and activate both genomic and nongenomic signaling pathways. *Am. J. Physiol. Lung Cell. Mol. Physiol.* **286**, L694–L700
29. Yu, J. J., Robb, V. A., Morrison, T. A., Ariazi, E. A., Karbowniczek, M., Astrinidis, A., et al. (2009) Estrogen promotes the survival and pulmonary metastasis of tuberin-null cells. *Proc. Natl. Acad. Sci. U. S. A.* **106**, 2635–2640
30. Lim, S. D., Stallcup, W., Lefkove, B., Govindarajan, B., Au, K. S., Northrup, H., et al. (2007) Expression of the neural stem cell markers NG2 and L1 in human angiomyolipoma: are angiomyolipomas neoplasms of stem cells? *Mol. Med.* **13**, 160–165
31. Vaughan, R. M., Kordich, J. J., Chan, C.-Y., Sasi, N. K., Celano, S. L., Sisson, K. A., et al. (2022) Chemical biology screening identifies a vulnerability to checkpoint kinase inhibitors in TSC2-deficient renal angiomyolipomas. *Front. Oncol.* **12**, 852859
32. Wu, G., Xing, M., Mambo, E., Huang, X., Liu, J., Guo, Z., et al. (2005) Somatic mutation and gain of copy number of PIK3CA in human breast cancer. *Breast Cancer Res.* **7**, R609–R616
33. Rieckhoff, J., Meyer, F., Classen, S., Zielinski, A., Riepen, B., Wikman, H., et al. (2020) Exploiting chromosomal instability of PTEN-deficient triple-negative breast cancer cell lines for the sensitization against PARP1 inhibition in a replication-dependent manner. *Cancers (Basel)* **12**, 2809
34. Sarbassov, D. D., Ali, S. M., Kim, D.-H., Guertin, D. A., Latek, R. R., Erdjument-Bromage, H., et al. (2004) Rictor, a novel binding partner of mTOR, defines a rapamycin-insensitive and raptor-independent pathway that regulates the cytoskeleton. *Curr. Biol.* **14**, 1296–1302
35. Schreiber, K. H., Ortiz, D., Academia, E. C., Anies, A. C., Liao, C.-Y., and Kennedy, B. K. (2015) Rapamycin-mediated mTORC2 inhibition is determined by the relative expression of FK506-binding proteins. *Aging Cell* **14**, 265–273
36. Sarbassov, D. D., Ali, S. M., Sengupta, S., Sheen, J.-H., Hsu, P. P., Bagley, A. F., et al. (2006) Prolonged rapamycin treatment inhibits mTORC2 assembly and Akt/PKB. *Mol. Cell* **22**, 159–168
37. Rozengurt, E., Soares, H. P., and Sinnet-Smith, J. (2014) Suppression of feedback loops mediated by PI3K/mTOR induces multiple overactivation of compensatory pathways: an unintended consequence leading to drug resistance. *Mol. Cancer Ther.* **13**, 2477–2488
38. Asih, P. R., Prikas, E., Stefanoska, K., Tan, A. R. P., Ahel, H. I., and Ittner, A. (2020) Functions of p38 MAP kinases in the central nervous system. *Front. Mol. Neurosci.* **13**, 570586
39. Anton, D. B., Ducati, R. G., Timmers, L. F. S. M., Laufer, S., and Goettert, M. I. (2021) A special view of what was almost forgotten: P38δ MAPK. *Cancers (Basel)* **13**, 2077
40. Tan, F. L.-S., Ooi, A., Huang, D., Wong, J. C., Qian, C.-N., Chao, C., et al. (2010) p38delta/MAPK13 as a diagnostic marker for cholangiocarcinoma and its involvement in cell motility and invasion. *Int. J. Cancer* **126**, 2353–2361
41. Escós, A., Risco, A., Alsina-Beauchamp, D., and Cuenda, A. (2016) p38γ and p38δ mitogen activated protein kinases (MAPKs), new stars in the MAPK galaxy. *Front. Cell Dev. Biol.* **4**, 31
42. Enslin, H., Brancho, D. M., and Davis, R. J. (2000) Molecular determinants that mediate selective activation of p38 MAP kinase isoforms. *EMBO J.* **19**, 1301–1311
43. Yang, C., Zhu, Z., Tong, B. C.-K., Iyaswamy, A., Xie, W.-J., Zhu, Y., et al. (2020) A stress response p38 MAP kinase inhibitor SB202190 promoted TFEB/TFE3-dependent autophagy and lysosomal biogenesis independent of p38. *Redox Biol.* **32**, 101445
44. Ke, S., Alemu, E. A., Mertens, C., Gantman, E. C., Fak, J. J., Mele, A., et al. (2015) A majority of m6A residues are in the last exons, allowing the potential for 3' UTR regulation. *Genes Dev.* **29**, 2037–2053
45. Liu, J., Li, K., Cai, J., Zhang, M., Zhang, X., Xiong, X., et al. (2020) Landscape and regulation of m6A and m6Am methylome across human and mouse tissues. *Mol. Cell* **77**, 426–440.e6
46. Park, O. H., Ha, H., Lee, Y., Boo, S. H., Kwon, D. H., Song, H. K., et al. (2019) Endoribonucleolytic cleavage of m6A-containing RNAs by RNase P/MRP complex. *Mol. Cell* **74**, 494–507.e8
47. Du, H., Zhao, Y., He, J., Zhang, Y., Xi, H., Liu, M., et al. (2016) YTHDF2 destabilizes m6A-containing RNA through direct recruitment of the CCR4-NOT deadenylase complex. *Nat. Commun.* **7**, 12626
48. Shyu, A. B., Greenberg, M. E., and Belasco, J. G. (1989) The c-fos transcript is targeted for rapid decay by two distinct mRNA degradation pathways. *Genes Dev.* **3**, 60–72
49. Kenney, J. W., Moore, C. E., Wang, X., and Proud, C. G. (2014) Eukaryotic elongation factor 2 kinase, an unusual enzyme with multiple roles. *Adv. Biol. Regul.* **55**, 15–27
50. Carlberg, U., Nilsson, A., and Nygård, O. (1990) Functional properties of phosphorylated elongation factor 2. *Eur. J. Biochem.* **191**, 639–645
51. Knebel, A., Morrice, N., and Cohen, P. (2001) A novel method to identify protein kinase substrates: eEF2 kinase is phosphorylated and inhibited by SAPK4/p38delta. *EMBO J.* **20**, 4360–4369
52. Smith, E. M., and Proud, C. G. (2008) cdc2-cyclin B regulates eEF2 kinase activity in a cell cycle- and amino acid-dependent manner. *EMBO J.* **27**, 1005–1016

mTORC1 suppresses progrowth signaling by RNA methylation

53. Wang, X., Li, W., Williams, M., Terada, N., Alessi, D. R., and Proud, C. G. (2001) Regulation of elongation factor 2 kinase by p90(RSK1) and p70 S6 kinase. *EMBO J.* **20**, 4370–4379
54. Yurtsever, Z., Patel, D. A., Kober, D. L., Su, A., Miller, C. A., Romero, A. G., et al. (2016) First comprehensive structural and biophysical analysis of MAPK13 inhibitors targeting DFG-in and DFG-out binding modes. *Biochim. Biophys. Acta* **1860**, 2335–2344
55. Bouhaddou, M., Memon, D., Meyer, B., White, K. M., Rezelj, V. V., Correa Marrero, M., et al. (2020) The global phosphorylation landscape of SARS-CoV-2 infection. *Cell* **182**, 685–712.e19
56. Hsieh, A. C., Nguyen, H. G., Wen, L., Edlind, M. P., Carroll, P. R., Kim, W., et al. (2015) Cell type-specific abundance of 4EBP1 primes prostate cancer sensitivity or resistance to PI3K pathway inhibitors. *Sci. Signal.* **8**, ra116
57. Melick, C. H., and Jewell, J. L. (2020) Small molecule H89 renders the phosphorylation of S6K1 and AKT resistant to mTOR inhibitors. *Biochem. J.* **477**, 1847–1863
58. Carracedo, A., Ma, L., Teruya-Feldstein, J., Rojo, F., Salmena, L., Alimonti, A., et al. (2008) Inhibition of mTORC1 leads to MAPK pathway activation through a PI3K-dependent feedback loop in human cancer. *J. Clin. Invest.* **118**, 3065–3074
59. Mendoza, M. C., Er, E. E., and Blenis, J. (2011) The Ras-ERK and PI3K-mTOR pathways: cross-talk and compensation. *Trends Biochem. Sci.* **36**, 320–328
60. Lu, Y., Zhang, E. Y., Liu, J., and Yu, J. J. (2020) Inhibition of the mechanistic target of rapamycin induces cell survival via MAPK in tuberous sclerosis complex. *Orphanet J. Rare Dis.* **15**, 209
61. Linares, J. F., Duran, A., Reina-Campos, M., Aza-Blanc, P., Campos, A., Moscat, J., et al. (2015) Amino acid activation of mTORC1 by a PB1-domain-driven kinase complex cascade. *Cell Rep.* **12**, 1339–1352
62. Jiang, Y., Gram, H., Zhao, M., New, L., Gu, J., Feng, L., et al. (1997) Characterization of the structure and function of the fourth member of p38 group mitogen-activated protein kinases, p38delta. *J. Biol. Chem.* **272**, 30122–30128
63. Henske, E. P., Jóźwiak, S., Kingswood, J. C., Sampson, J. R., and Thiele, E. A. (2016) Tuberous sclerosis complex. *Nat. Rev. Dis. Primers* **2**, 16035
64. Liu, Y., Chang, Y., and Cai, Y. (2020) circTNRSF21, a newly identified circular RNA promotes endometrial carcinoma pathogenesis through regulating miR-1227-MAPK13/ATF2 axis. *Aging (Albany N.Y.)* **12**, 6774–6792
65. Parkhitko, A. A., Priolo, C., Coloff, J. L., Yun, J., Wu, J. J., Mizumura, K., et al. (2014) Autophagy-dependent metabolic reprogramming sensitizes TSC2-deficient cells to the antimetabolite 6-aminonicotinamide. *Mol. Cancer Res.* **12**, 48–57
66. Tang, Y., Kwiatkowski, D. J., and Henske, E. P. (2022) Midkine expression by stem-like tumor cells drives persistence to mTOR inhibition and an immune-suppressive microenvironment. *Nat. Commun.* **13**, 5018
67. Atochina-Vasserman, E. N., Abramova, E., James, M. L., Rue, R., Liu, A. Y., Ersumo, N. T., et al. (2015) Pharmacological targeting of VEGFR signaling with axitinib inhibits Tsc2-null lesion growth in the mouse model of lymphangioliomyomatosis. *Am. J. Physiol. Lung Cell. Mol. Physiol.* **309**, L1447–L1454